# Automatic Control of Aircraft in Lateral-Directional Plane During Landing

Romulus Lungu[1], Mihai Lungu[2]

[1] University of Craiova, Faculty of Electrical Engineering, 107 Decebal Blvd., Craiova, Romania, rlungu@elth.ucv.ro
[2] University of Craiova, Faculty of Electrical Engineering, 107 Decebal Blvd., Craiova, Romania, Lma1312@yahoo.com

The paper focuses on the automatic control of aircraft in the lateral-directional plane, during the landing approach phase, taking into consideration the crosswind and the sensors' errors. Two new automatic landing systems are designed by using the H-inf control, the dynamic inversion, optimal observers, and reference models. To validate them, we use the dynamics associated to the landing of a light airplane, we software implement the theoretical results, and we analyze the accuracy of the results and the precision standards' achievement with respect to the requirements of the Federal Aviation Administration for the lateral error during the lateral-directional motion of the aircraft during landing approach phase.

**Key words:** Lateral-directional motion, Landing, H-inf control, Dynamic inversion, Observer

## 1. Introduction

*A. Antecedents and motivations*

The Automatic Landing Systems (ALSs) are used for aicraft landing control; among the first such systems there can be mentioned the ones tested in September 1947, allowing the complete fully automatic takeoff and landing. The main three phases in a typical landing procedure (longitudinal plane) are: the initial approach, the glide slope, and the flare [1-4]. Firstly, during the initial approach, the pilot must cancel the aicraft lateral deviation with respect to the runway; meanwhile, the pilot descends from the cruise altitude to an altitude of approximately 400 m above the ground for heavy aircraft or less than 400 m for light aircraft. The pilot then positions the airplane so that it is on a heading towards the runway centerline. When the aircraft approaches the outer airport marker, which is about 4 nautical miles from the runway, the glide slope path signal is intercepted. As the airplane descends along the glide slope path, its pitch, attitude, and speed must be controlled; the aircraft maintains a constant speed along the flight path. The landing approach phase of flight is perhaps the most critical phase for medium weight class airplanes. The airplane must be characterized by good handling qualities in order not to unnecessarily add to the pilot's workload during this phase of landing. The landing approach phase requires accurate positioning of the airplane relative to the runway with a limited margin for error.

In the ALSs' design process, one can use different conventional control laws as: proportional-derivative (PD), proportional-integral (PI), proportional-integral-derivative (PID) for the altitude and descent velocity control [1-3], PD or PID conventional laws for the pitch angle and pitch rate control, as well as different laws based on the state vector, dynamic inversion concept, with command filters, dynamic compensators, and state observers [4-7]. There are also used the optimal synthesis $H_2$, $H_\infty$, $H_2/H_\infty$ [8], the adaptive synthesis based on dynamic inversion theory and neural networks theory [9, 10], or fuzzy techniques [11, 12]. In the research area of optimal synthesis, Shue and Agarwal [13] have developed a mixed technique for the $H_2/H_\infty$ control of the landing, while Ochi and Kanai [14] have used the $H_\infty$ control technique to design aircraft automatic approach and landing. In these papers, the authors did not analyze the robustness of the designed controllers in the presence of sensor errors and crosswind (lateral wind) – issue which is considered in our paper. This is achieved in [15], where a PD-type fuzzy control system is developed for automatic landing control of both linear and nonlinear aircraft model. The drawback is that the authors only set up the wind disturbance as the initial condition; persistent wind disturbance is not considered. The learning scheme using fuzzy controllers with the Back-propagation Through Time (BPTT), presented in [16], guides the aircraft to a

safe landing and makes the controller more robust and adaptive to the ever-changing environment. To design systems for the landing control in lateral-directional plane, different techniques are available: H-inf control, linear quadratic optimal control (LQR/LQG), and structured singular value μ-synthesis. The study [17] did not include weather factors such as wind disturbances; same conclusions can be drawn from the work of Singh and Padhi [2] where a nonlinear control has been designed by using the dynamic inversion approach for the automatic landing of unmanned aerial vehicles along with the associated path planning. The obtained algorithm is not tested in the presence of crosswind and/or wind gusts, this being a disadvantage of the algorithm. An alternative of the above presented control techniques can be the usage of neural networks; the disadvantage of these systems is related to the flight path track accuracy; for example, the time delay neural network controller designed in [18] is enable only under limited conditions. If severe wind disturbances are encountered, the pilot must handle the aircraft due to the limits of the automatic landing system.

*B. Main contribution*

This paper focuses on the automatic control of aircraft in the lateral-directional plane, during landing approach phase, by using the linearized lateral dynamics of aircraft, the H-inf control, and the dynamic inversion concept, taking into consideration the crosswind and the errors of the sensors. Our aim is to design new landing flight control systems in lateral-directional plane which cancel the negative effect of crosswind and sensors' errors, which can be used with good results when the number of sensors is smaller than the number of states that must be known, and which can handle the situations when the actuators' dynamics is nonlinear, without using neural networks due to their limited conditions of functionality. According to this paper's authors, little progress has been reported for the landing flight control systems in the lateral-directional plane (using the H-inf control and the dynamic inversion) handling all the above presented problems; this motivates the present study.

The systems designed in this paper represent extensions of the automatic landing system presented in [4], where only the landing in longitudinal plane is analyzed. Our systems differ from other similar automatic landing systems from the specialty literature, being designed for the lateral-directional motion of the aircraft during landing approach phase; with some changes, the systems can be used for the control of landing in the longitudinal (vertical) plane or for other flight trajectories. Our new ALSs have some additional elements with respect to the one presented in [4]: 1) two reference models which provide the aircraft desired lateral deviation, sideslip angle, and their derivatives up to relative degrees of the systems; 2) an optimal observer which is used for the estimation of the error $\Delta\hat{x} = \hat{x} - \bar{x}$ ($\bar{x}$ is the aircraft desired state, while $\hat{x}$ is the estimated state) in the presence of crosswind and sensor error; 3) a dynamic compensator (only for the second designed ALS) which provides one of the control law components (the pseudo-command signal). By using the states of the reference models, we calculate $\bar{x}$ and the reference vector $(\bar{y})$ for the measured output *y*. The optimal control is made on-line after the deviation (error) $\Delta\hat{x}$. The inputs of the reference models are the reference lateral deviation and the sideslip angle (calculated for the landing approach phase). By means of the two reference models' states, one calculates the desired component $\bar{u}$ (guidance component) of the control laws for the imposed lateral-directional trajectory by using the dynamic inversion approach in two variants. The other component of the control laws $(u_\infty)$ is determined by using the H-inf method. The two calculation methods for $\bar{u}$ differ from the one presented in [4] especially by a greater degree of generality, applicability, and simplicity; the control law presented in [4] consists of separating the controller in two subsystems: a stable one and an unstable one which must be stabilized separately, this leading to a more complicated design procedure.

## 2. Aircraft Dynamics in Lateral-Directional Plane during Landing

As we already mentioned, aircraft landing is simplified if the motion of the aircraft in lateral plane is made without errors (deviation of the aircraft from the runway direction is zero). This is why the system for the automatic control of the flight direction is very important. Before the start of the landing two main stages in longitudinal plane (the glide slope phase and the flare phase), the pilot must cancel the aircraft

lateral deviation with respect to the runway. This can be achieved by means of the automatic control systems designed in this paper or by using other control systems for the flight direction control with radio navigation subsystem and equipment for the measurement of the distance between the aircraft and the radio markers [15, 19, 20, 21, 22].

The linearization of an aircraft nonlinear dynamics is generally based on the method of small disturbances with respect to an equilibrium trajectory. The general linear model of the aircraft motion (**A**), in lateral-directional plane, is described by the equations [5]:

$$\dot{\beta} = a_{11}\beta + a_{12}p + a_{13}r + a_{14}\varphi + b_{11}\delta_a + b_{12}\delta_r + \frac{a_{11}}{V_0}V_{vy},\ \dot{p} = a_{21}\beta + a_{22}p + a_{23}r + b_{21}\delta_a + b_{22}\delta_r + \frac{a_{21}}{V_0}V_{vy},$$

$$\dot{r} = a_{31}\beta + a_{32}p + a_{33}r + b_{31}\delta_a + b_{32}\delta_r + \frac{a_{31}}{V_0}V_{vy},\ \dot{\varphi} = p,\ \dot{\psi} = r,\ \dot{Y} = -V_0\beta + V_0\psi + V_{vy}, \quad (1)$$

$$\dot{\delta}_a = -\frac{1}{T_a}\delta_a + \frac{1}{T_a}\delta_{a_c},\ \dot{\delta}_r = -\frac{1}{T_r}\delta_r + \frac{1}{T_r}\delta_{r_c},$$

where $\beta$ is the aircraft sideslip angle, $\varphi$ and $\psi$ are the roll angle and the yaw angle, respectively, $p$ – the aircraft roll angular rate, $r$ – the aircraft yaw angular rate, $Y$ – the deviation of the aircraft with respect to the runway direction, $\delta_a$ and $\delta_r$ – the deflection angles of the ailerons and rudder, respectively, $\delta_{a_c}$ and $\delta_{r_c}$ – the roll and yaw commands (commands applied to the actuators), $V_{vy}$ – the component of the wind velocity along the lateral axis of the aircraft, $V_0$ – aircraft nominal velocity, $T_a$ and $T_r$ – the effectors' time delay constants of the ailerons and rudder, respectively. Aircraft's lateral motion may be written under the form:

$$\dot{x} = Ax + Bu + Gw; \quad (2)$$

here $x$ is the state vector, $u$ - the command vector, while the crosswind $w = V_{vy}$ is the system's disturbance which is estimated by the equipment from aircraft's navigation system; the forms of $x$ and $u$ are $x = [\beta \quad p \quad r \quad \varphi \quad \psi \quad Y \quad \delta_a \quad \delta_r]^T$ and $u = [\delta_{a_c} \quad \delta_{r_c}]^T$, respectively.

By identification of equations (1) and (2), we obtain the matrices $A \in R^{8\times 8}$, $B \in R^{8\times 2}$, and $G \in R^{8\times 1}$;

$$A = \begin{bmatrix} a_{11} & a_{12} & a_{13} & a_{14} & 0 & 0 & b_{11} & b_{12} \\ a_{21} & a_{22} & a_{23} & 0 & 0 & 0 & b_{21} & b_{22} \\ a_{31} & a_{32} & a_{33} & 0 & 0 & 0 & b_{31} & b_{32} \\ 0 & 1 & 0 & 0 & 0 & 0 & 0 & 0 \\ 0 & 0 & 1 & 0 & 0 & 0 & 0 & 0 \\ -V_0 & 0 & 0 & 0 & V_0 & 0 & 0 & 0 \\ 0 & 0 & 0 & 0 & 0 & 0 & -\frac{1}{T_a} & 0 \\ 0 & 0 & 0 & 0 & 0 & 0 & 0 & -\frac{1}{T_r} \end{bmatrix}, B = \begin{bmatrix} 0 & 0 \\ 0 & 0 \\ 0 & 0 \\ 0 & 0 \\ 0 & 0 \\ 0 & 0 \\ \frac{1}{T_a} & 0 \\ 0 & \frac{1}{T_r} \end{bmatrix}, G = \begin{bmatrix} \frac{a_{11}}{V_0} \\ \frac{a_{21}}{V_0} \\ \frac{a_{31}}{V_0} \\ 0 \\ 0 \\ 1 \\ 0 \\ 0 \end{bmatrix}. \quad (3)$$

## 3. Design of the First Flight Control System for the Landing Approach Phase

### *A. Problem formulation*

Optimal control problems have became more and more important in the design of modern engineering systems [23]. The solving of an optimal problem means the determining of a system input which optimizes a given cost functional [24]; the control input that yields an extreme of the cost functional is known as the optimal control and the corresponding variation of the state variables is called the optimal trajectory. The first flight control system presented in this paper may be used mainly during the landing approach phase, but, changing aircraft's dynamics and the controlled variables, it can also be a solution for the aircraft control in

longitudinal plane during the two main phases: the glide slope and the flare.

For the design of this first control system, let us consider the vector $z = \begin{bmatrix} Y & \beta \end{bmatrix}^T = C'x$ containing the system's controllable output variables and the vector $\bar{z} = \begin{bmatrix} \bar{Y} & \bar{\beta} \end{bmatrix}^T$ containing the system's reference variables (the imposed values of aircraft's lateral deviation and sideslip angle). The system's output vector is *y*, chosen of the form: $y = \begin{bmatrix} Y & \dot{Y} & \beta & \varphi & p & \psi & r \end{bmatrix}^T = Cx$; the sensors' errors have been not taken into account here. The matrices $C \in R^{7\times 8}$ and $C' \in R^{2\times 8}$ are respectively:

$$C = \begin{bmatrix} 0 & 0 & 0 & 0 & 0 & 1 & 0 & 0 \\ -V_0 & 0 & 0 & 0 & V_0 & 0 & 0 & 0 \\ 1 & 0 & 0 & 0 & 0 & 0 & 0 & 0 \\ 0 & 0 & 0 & 1 & 0 & 0 & 0 & 0 \\ 0 & 1 & 0 & 0 & 0 & 0 & 0 & 0 \\ 0 & 0 & 0 & 0 & 1 & 0 & 0 & 0 \\ 0 & 0 & 1 & 0 & 0 & 0 & 0 & 0 \end{bmatrix}, C' = \begin{bmatrix} 0 & 1 \\ 0 & 0 \\ 0 & 0 \\ 0 & 0 \\ 0 & 0 \\ 1 & 0 \\ 0 & 0 \\ 0 & 0 \end{bmatrix}^T . \quad (4)$$

The command law is calculated by using the formula:

$$u = \bar{u} + u_\infty , \quad (5)$$

where $u_\infty$ is the optimal command calculated by means of the H-inf method, while the component $\bar{u}$ is calculated by using the dynamic inversion; $u_\infty$ will be obtained in the next sub-section, while the component $\bar{u}$ will be designed in section 3.C. For the design of signal $\bar{u}$, there will be used the dynamic inversion principle and the vectors $\bar{z} = C'\bar{x}$, $\bar{y} = C\bar{x}$, where $\bar{x}$ is determined from the equation $\dot{\bar{x}} = A\bar{x} + B\bar{u}$.

*B. Design of the first component ($u_\infty$) of the control law u*

The state equation (2), the equations associated to $z_1$=*Y* and $z_2$=β, as well as the equation of the output vector *y*, may be combined into the following equation:

$$\begin{bmatrix} \dot{x} \\ z_1 \\ z_2 \\ y \end{bmatrix} = \begin{bmatrix} A_{(8\times 8)} & B_{(8\times 2)} & G_{(8\times 1)} & 0_{(8\times 7)} \\ C_{0\,(1\times 8)} & D_{01(1\times 2)} & 0_{(1\times 1)} & 0_{(1\times 7)} \\ C_{1(1\times 8)} & D_{11(1\times 2)} & 0_{(1\times 1)} & 0_{(1\times 7)} \\ C_{(7\times 8)} & 0_{(7\times 2)} & 0_{(7\times 1)} & D_{22(7\times 7)} \end{bmatrix} \begin{bmatrix} x \\ u \\ w \\ e \end{bmatrix}; \quad (6)$$

the matrices $A, B, G$ have the forms (3) and $C_0 = \begin{bmatrix} 0 & 0 & 0 & 0 & 0 & 1 & 0 & 0 \end{bmatrix}, C_1 = \begin{bmatrix} 1 & 0 & 0 & 0 & 0 & 0 & 0 & 0 \end{bmatrix}, D_{01} = \begin{bmatrix} c_1 & 0 \end{bmatrix}, D_{11} = \begin{bmatrix} 0 & c_2 \end{bmatrix}$; the matrix *C* has the form given in (4), while $D_{22}=I_7$ for the vector containing the sensor errors: $e = \begin{bmatrix} e_Y & e_{\dot{Y}} & e_\beta & e_\varphi & e_p & e_\psi & e_r \end{bmatrix}^T$. It is known that the sensors (used to measure some important variables) have sometimes errors; for example, the most important errors of a gyro sensor are: 1) the bias; 2) the scale factor; 3) the calibration error of the scale factor; 4) the noise of the sensor; 5) the sensibility to an acceleration applied along an arbitrary direction. The bias and the noise are the most severe for the control performance during landing. Usually, on aircraft there are used giros to measure the angular rates (in our case *p* and *r*); by integration of the obtained values, the roll and yaw angles result. Moreover, on aircraft there are transducers (sensors) for the attack angle and for the sideslip angle (β). Therefore, in this paper, we considered sensor errors for β, *p*, and *r*. The general model of the gyro sensor is the one in [1]. In the software implemnetation of the two automatic landing systems (section 5), the authors will use some information from [1], but will increase considerably the values of the sensors' errors to study the robustness of the two ALSs. To proof that, in steady regime, the forms of $z_1$=*Y* and $z_2$=β are the same with the ones in (6), one has used the expansion of $z = \begin{bmatrix} z_1 & z_2 \end{bmatrix}^T$ as function of state (*x*) and of the system command vector

($u$); for $u_0$=0, one succesively obtained: $z=\begin{bmatrix} z_1 \\ z_2 \end{bmatrix}=z(x,u)\cong \underbrace{z(x_0,u_0)}_{z_0}+\left(\frac{\partial z}{\partial x}\right)_{(x_0,0)}\Delta x+\left(\frac{\partial z}{\partial u}\right)_{(x_0,0)}\Delta u\cong z_0+$

$+\underbrace{\begin{bmatrix} \frac{\partial z_1}{\partial x_1} & \cdots & \frac{\partial z_1}{\partial x_n} \\ \frac{\partial z_2}{\partial x_1} & \cdots & \frac{\partial z_2}{\partial x_n} \end{bmatrix}_{(x_0,0)}}_{\begin{bmatrix} C_0 \\ C_1 \end{bmatrix}}\Delta x+\underbrace{\begin{bmatrix} \frac{\partial z_1}{\partial u_1} & \frac{\partial z_1}{\partial u_2} \\ \frac{\partial z_2}{\partial u_1} & \frac{\partial z_2}{\partial u_2} \end{bmatrix}_{(x_0,0)}}_{\begin{bmatrix} D_{01} \\ D_{11} \end{bmatrix}}\Delta u \Leftrightarrow \Delta z\cong\begin{bmatrix} C_0 \\ C_1 \end{bmatrix}\Delta x+\begin{bmatrix} D_{01} \\ D_{11} \end{bmatrix}\Delta u \Leftrightarrow z\cong\begin{bmatrix} C_0 \\ C_1 \end{bmatrix}x+\begin{bmatrix} D_{01} \\ D_{11} \end{bmatrix}u\cong \overline{C}\,x+\overline{D}u,$

where $C_0=\begin{bmatrix} \frac{\partial z_1}{\partial x_1} & \cdots & \frac{\partial z_1}{\partial x_n} \end{bmatrix}_{(x_0,0)}, C_1=\begin{bmatrix} \frac{\partial z_2}{\partial x_1} & \cdots & \frac{\partial z_2}{\partial x_n} \end{bmatrix}_{(x_0,0)}$; $x_i\left(i=\overline{1,n}\right)$ are the state of the system ($n$=8), $D_{01}=\begin{bmatrix} \frac{\partial Y}{\partial \delta_{a_c}} & \frac{\partial Y}{\partial \delta_{r_c}} \end{bmatrix}_{(x_0,0)}=\begin{bmatrix} c_1 & 0 \end{bmatrix}, D_{11}=\begin{bmatrix} \frac{\partial z_2}{\partial u_1} & \frac{\partial z_2}{\partial u_2} \end{bmatrix}_{(x_0,0)}=\begin{bmatrix} \frac{\partial \beta}{\partial \delta_{a_c}} & \frac{\partial \beta}{\partial \delta_{r_c}} \end{bmatrix}_{(x_0,0)}=\begin{bmatrix} 0 & c_2 \end{bmatrix}$, $\overline{C}=\begin{bmatrix} C_0 \\ C_1 \end{bmatrix}, \overline{D}=\begin{bmatrix} D_{01} \\ D_{11} \end{bmatrix}$. $c_1$ and $c_2$ have small positive values; in steady regime ($u$=0), one gets $z_1$=$Y$ and $z_2$=β.

The optimal control law has the form [1]:

$$u_\infty=-K_\infty(\hat{x}-\bar{x}), K_\infty=R_1^{-1}B^TP_\infty, R_1=\overline{D}^T\overline{D}; \tag{7}$$

$u_\infty$ must minimize the cost functional $J=\frac{1}{2}\int_0^\infty z^Tz\mathrm{d}t=\frac{1}{2}\int_0^\infty\left[x^T\underbrace{\left(\overline{C}^T\overline{C}\right)}_{Q_1}x+u_\infty^T\underbrace{\left(\overline{D}^T\overline{D}\right)}_{R_1}u_\infty\right]\mathrm{d}t$. The symmetric and positive defined matrix $P_\infty\in R^{8\times8}$ is the stabilizing solution of the Riccati matriceal equation [13]

$$A^TP_\infty+P_\infty A-P_\infty\left(BR_1^{-1}B^T-\mu_1^{-2}GG^T\right)P_\infty+Q_1=0. \tag{8}$$

Here, $R_1$ must be a positive defined matrix, while $\mu_1$ is a small enough positive scalar for which the Riccati equation (8) has a stabilizing solution. The determination of the controller gain matrix $(K_\infty)$ is the so-called H-inf control problem. The plant inputs are classified as control inputs and disturbances. The control input ($u$) is the output of the controller, which becomes the input to the actuators driving the system (aircraft). Disturbances $w$=$V_{vy}$ and $e$ are called exogenous inputs; the main distinction between the control input and the exogenous inputs is that the controller can not manipulate exogenous inputs. The plant's outputs are also characterized into two groups; the first group is represented by signals that are measured and become inputs of the controller; the second group is represented here by the performance outputs ($z_1$ and $z_2$). In this paper, one will not insist on this whole theory since it is well presented in many papers [13, 14, 25]. It can only be noted that the H-inf control problem means to find a controller for the generalized plant such that the infinity norm of the transfer function relating exogenous inputs to performance outputs is minimum. The controller gain matrix $(K_\infty)$ has the general form (7) which is typical for the optimal control theory. The optimal control law $u_\infty$ depends on $\Delta\hat{x}=\hat{x}-\bar{x}$, as one can see in (7). To obtain this signal, an ordinary observer must be used; here, in order to obtain the estimated state vector $(\hat{x})$ and the signal $\Delta\hat{x}=\hat{x}-\bar{x}$, one borrowed the observer presented in [25], i.e.: $\Delta\dot{\hat{x}}=A\Delta\hat{x}+Bu+L_\infty(\Delta y-C\Delta\hat{x})$. $w=V_{vy}$ is estimated by means of the equipment from the navigation system. The observer gain matrix $L_\infty\in R^{8\times7}$ is calculated by using the formula: $L_\infty=P_\infty^*C^T\left(D_{22}^TD_{22}\right)^{-1}$, with $P_\infty^*-$ the stabilizing solution of the Riccati matriceal equation [13]:

$$AP_\infty^*+P_\infty^*A^T-P_\infty^*\left(C^TC-\mu_2^{-2}\overline{C}^T\overline{C}\right)P_\infty^*+GG^T=0; \tag{9}$$

$\mu_2$ is a small enough positive scalar for which the Riccati equation (9) has a stabilizing solution.

*C. Design of the second component (guidance component - $\bar{u}$) of the control law u*

First, we will obtain the relative degrees of the variables $z_1$=$Y$ and $z_2$=β; these relative degrees will be

denoted here with $r_1$ and $r_2$, respectively. We derivate with respect to time the equations associated to $Y$ and $\beta$ ($r_1$ times and $r_2$ times, respectively) until the components of the command vector $u$, i.e. $\delta_{a_c}$ and $\delta_{r_c}$, are obtained; the following equations have resulted:

$$\begin{aligned}
\ddot{Y} &= a'_{61}\beta + a'_{62}p + a'_{63}r + a'_{64}\varphi + a'_{67}\delta_a + a'_{68}\delta_r - \frac{V_0 b_{11}}{T_a}\delta_{a_c} - \frac{V_0 b_{12}}{T_r}\delta_{r_c} + (a_{31} - a'_{11})V_{vy} - a_{11}\dot{V}_{vy}, \\
\ddot{\beta} &= a'_{11}\beta + a'_{12}p + a'_{13}r + a'_{14}\varphi + a'_{17}\delta_a + a'_{18}\delta_r + \frac{b_{11}}{T_a}\delta_{a_c} + \frac{b_{12}}{T_r}\delta_{r_c} + \frac{a'_{11}}{V_0}V_{vy} + \frac{a_{11}}{V_0}\dot{V}_{vy},
\end{aligned} \tag{10}$$

where

$$\begin{aligned}
&a'_{11} = a_{11}^2 + a_{12}a_{21} + a_{13}a_{31},\ a'_{12} = a_{11}a_{12} + a_{12}a_{22} + a_{13}a_{32} + a_{14},\ a'_{13} = a_{11}a_{13} + a_{12}a_{23} + a_{13}a_{33},\ a'_{14} = a_{11}a_{14}, \\
&a'_{17} = a_{11}b_{11} + a_{12}b_{21} + a_{13}b_{31} - b_{11}/T_a,\ a'_{18} = a_{11}b_{12} + a_{12}b_{22} + a_{13}b_{32} - b_{12}/T_r,\ a'_{61} = V_0(a_{31} - a'_{11}), \\
&a'_{62} = V_0(a_{32} - a'_{12}),\ a'_{63} = V_0(a_{33} - a'_{13}),\ a'_{64} = -V_0 a'_{14},\ a'_{67} = V_0(b_{31} - a'_{17}),\ a'_{68} = V_0(b_{32} - a'_{18}),\ a'_{31} = a_{31} - a'_{11}.
\end{aligned} \tag{11}$$

Thus, according to equations (10), the relative degrees are $r_1$=3 and $r_2$=2. The equations (10) may be combined in the equation of the vector $z^{(r)} = \left[\ddot{Y}\ \ddot{\beta}\right]^T$, i.e.:

$$z^{(r)} = A_x x + B_u \bar{u} + G'\tilde{w}, \tag{12}$$

where $\bar{u} = \left[\bar{\delta}_{a_c}\ \ \bar{\delta}_{r_c}\right]^T$, $\tilde{w} = \left[V_{vy}\ \ \dot{V}_{vy}\right]^T$, $A_x = \begin{bmatrix} a'_{61} & a'_{62} & a'_{63} & a'_{64} & 0 & 0 & a'_{67} & a'_{68} \\ a'_{11} & a'_{12} & a'_{13} & a'_{14} & 0 & 0 & a'_{17} & a'_{18} \end{bmatrix}$, $B_u = \begin{bmatrix} -\frac{V_0 b_{11}}{T_a} & -\frac{V_0 b_{12}}{T_r} \\ \frac{b_{11}}{T_a} & \frac{b_{12}}{T_r} \end{bmatrix}$, $G' = \begin{bmatrix} a'_{31} & -a_{11} \\ -\frac{a'_{11}}{V_0} & \frac{a_{11}}{V_0} \end{bmatrix}$.

The form of the command law $\bar{u}$ results from (12) if we impose the convergence of $z^{(r)} = \left[\ddot{Y}\ \ddot{\beta}\right]^T$ to $\bar{z}^{(r)} = \left[\bar{\ddot{Y}}\ \bar{\ddot{\beta}}\right]^T$ and the convergence of the system estimated state $(\hat{x})$ to $x$; in these conditions, we get:

$$\bar{u} = B_u^{-1}\left(\bar{z}^{(r)} - A_x\hat{x} - G'\tilde{w}\right). \tag{13}$$

*D. The structure of the first new automatic landing system for the approach phase*

The structure of the first new control system for the aircraft guidance during landing approach phase, using dynamic inversion and H-inf method, is presented in Fig. 1. The vectors $\bar{z}$ and $\bar{z}^{(r)}$ are calculated by means of two reference models, the former being a three order reference model (associated to $Y$), while the latter is a second order reference model (associated to $\beta$) (Fig. 2) [5]; for the two reference models, to this first control system, we considered $v_{h_1} = v_{h_2} = 0$. The desired landing trajectory of aircraft mainly involves two variables' control: the aircraft lateral deviation with respect to the runway ($Y$) and the sideslip angle ($\beta$).

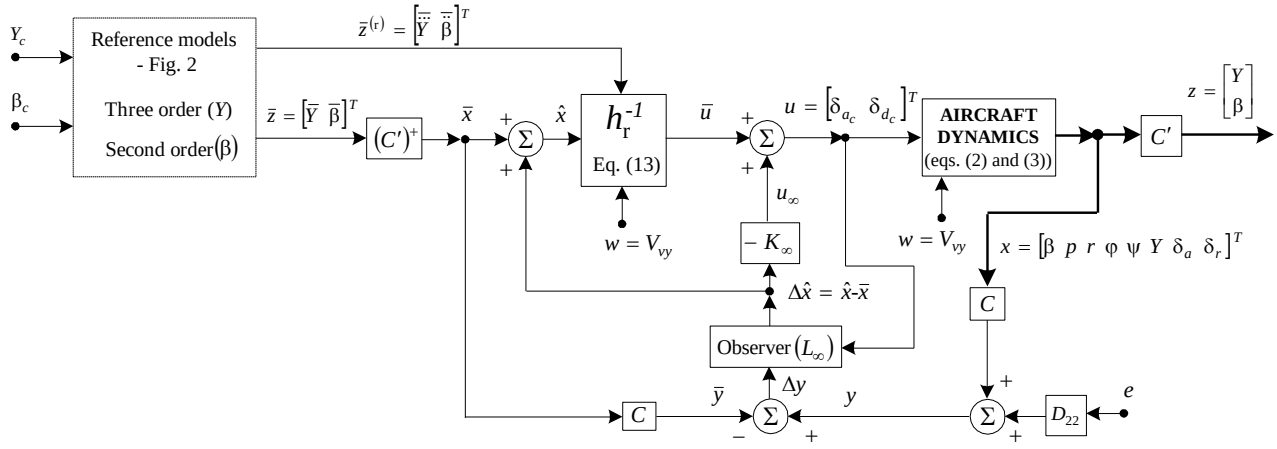


Fig. 1 The first ALS for the aircraft control in lateral plane using the H-inf control and the dynamic inversion

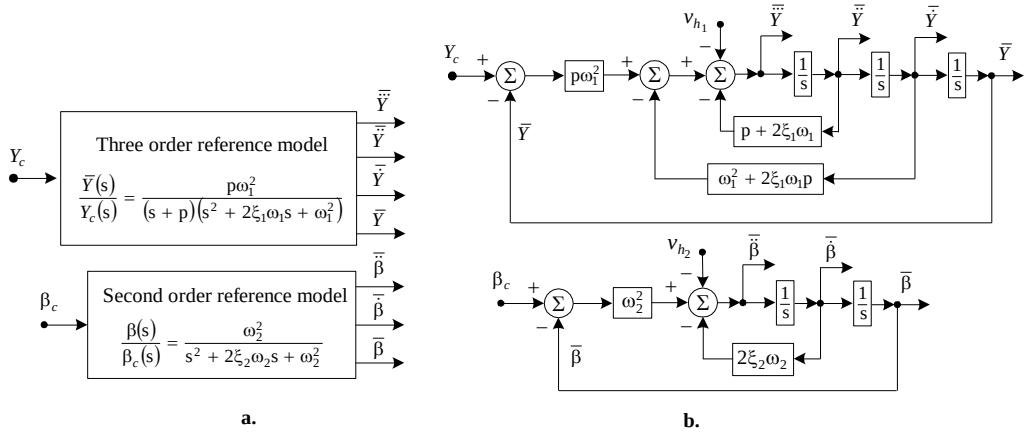


Fig. 2. Block diagrams of the three order and second order reference models, respectively: a) simplified block diagrams; b) detailed block diagrams

The dynamic inversion and H-inf method must assure the convergences: $\Delta y \to 0\,(y = Cx \to \bar{y} = C\bar{x},\, x \to \bar{x})$, $\Delta z \to 0\,(z = C'x \to \bar{z} = C'\bar{x}),\, \Delta\hat{x} \to 0\,(\hat{x} \to x \to \bar{x}),\, u_\infty \to 0,\, \bar{u} \to 0,\, u \to 0$.

## 4. Design of the Second Flight Control System for the Landing Approach Phase

Like the first landing system (presented in the third section), this second one is also used for the landing approach phase and for the aircraft's control in lateral-directional plane during the two main phases of a typical landing procedure in longitudinal plane. The main difference between the two control systems is the method used for the design of the control law *u*; other differences will be presented later in this section and in the fifth section of the paper. Like in the third section of the paper, the dynamic inversion and the H-inf control will be used again, this time, a dynamic compensator being integrated into the system; moreover, the design of the control law's first component $(u_\infty)$ is achieved again by means of the equations (6)-(8); it differs the method for the calculation of the second component (guidance component - $\bar{u}$) of the control law *u*. Also, a Pseudo Control Hedging (PCH) block will be inserted in the system to limit the pseudo-control by means of a component which represents the estimation error of the actuator's dynamics; the signal provided by PCH block represents a reference model additional input.

### *A. Design of the control law u*

We start the design of the control law *u* considering that a flying object's nonlinear dynamics, with one input (*u*) and one output (*z*), is generally described by the equations [26]:

$$\dot{x} = f(x, \bar{u}),\, z = h(x), \tag{14}$$

with $x(n\times 1)$ – the state vector, $n$ – the number of the state variables, $f$ and $h$ – nonlinear functions, generally unknown, $u$ and $z$ – the system's input and output vectors, respectively. In this paper, we assume that $h(x)$ is a uniquely invertible function. This dynamics satisfies the hypothesis in [27] and the equations:

$$z^{(r)} = h_r(x, \bar{u}),\, h_r = \frac{d^r h}{dt^r} = h^{(r)},\, \frac{\partial h_i}{\partial u} = 0,\, 0 \le i \le r,\, \frac{\partial h_r}{\partial u} \ne 0; \tag{15}$$

this means that all derivatives $z^{(i)} = h^{(i)}(x,u) = h^{(i)},\, i = \overline{0, r}$, do not depend on $\bar{u}$, while the derivative $z^{(r)} = h_r(x,\bar{u}) = h^{(r)}$ depends on $\bar{u}$; r is the relative degree of the system (14), while $z$ and $z^{(r)}$ are $z = [Y\ \beta]^T = [h_1(x)\ \ h_2(x)]^T$ and $z^{(r)} = \left[z_1^{(r_1)}\ \ z_2^{(r_2)}\right]^T = \left[\ddot{Y}\ \ddot{\beta}\right]^T = \left[h_1^{(r_1)}(x)\ \ h_2^{(r_2)}(x)\right]^T$, respectively; also, $r = r_1 + r_2$.

Denoting with $\hat{h}_r(z, \bar{u})$ – the best approximation of the function $h_r(x,u) = h_r(x(z), \bar{u}) = h_r(z, \bar{u})$, we design the control law (the pseudo-command):

$$\hat{v} = h_r(z, \hat{u}). \tag{16}$$

The equations (15) and (16) are equivalent with the following ones: $\bar{u} = h_{\mathrm{r}}^{-1}(z, v), \hat{u} = h_{\mathrm{r}}^{-1}(z, \hat{v})$; if $\hat{h}_{\mathrm{r}} = h_{\mathrm{r}}$, then, according to (15) and (16), one gets $z^{(\mathrm{r})} = v = \hat{v}$; otherwise,

$$z^{(\mathrm{r})} = \hat{v} + \varepsilon, \tag{17}$$

where $\varepsilon = \varepsilon(x, \bar{u}) = h_{\mathrm{r}}(z, \bar{u}) - \hat{h}_{\mathrm{r}}(z, \hat{u})$ is the approximation error of the function $h_{\mathrm{r}}$ (the inversion error), which acts like a disturbing signal of the system. Moreover, the equation (17) expresses the presence of *r* ideal integrators between the pseudo-command (pseudo-control) *v* and the output *z*. Imposing that $z \to \bar{z}, \dot{z} \to \dot{\bar{z}}, \ldots, z^{(\mathrm{r})} \to \bar{z}^{(\mathrm{r})}$, the signal *v* can be chosen of form [28]:

$$v = \hat{v} + \varepsilon = \bar{z}^{(\mathrm{r})} + \hat{v}_{pd} + \varepsilon; \tag{18}$$

$\hat{v}_{pd}$ is the output of the linear dynamic compensator, used for the control of the linear subsystem (17).

The linear system (17), having the input $v = \hat{v} + \varepsilon$ and the output *z*, is described by the transfer matrix $H_d(\mathrm{s}) = \mathrm{diag}\left\{H_{d_1}(\mathrm{s}), H_{d_2}(\mathrm{s})\right\}$, with $H_{d_i}(\mathrm{s}), i = \overline{1,2}$, having the forms: $H_{d_i}(\mathrm{s}) = \dfrac{b_{0i}}{\mathrm{s}^{\mathrm{r}_i} + \lambda_{\mathrm{r}_i - 1, i}\,\mathrm{s}^{\mathrm{r}_i - 1} + \ldots + \lambda_{1,i}\,\mathrm{s} + \lambda_{0i}}$.

Now, by using the notations:

$$\begin{aligned} Z &= \left[z \;\; \dot{z} \;\; \ldots \;\; z^{(\mathrm{r}-1)}\right]^T = \left[z_1 \;\; \dot{z}_1 \;\; \ddot{z}_1 \;\; z_2 \;\; \dot{z}_2\right]^T = \left[Y \;\; \dot{Y} \;\; \ddot{Y} \;\; \beta \;\; \dot{\beta}\right]^T, \\ \boldsymbol{\lambda} &= \begin{bmatrix} \boldsymbol{\lambda}_1 & 0_{\mathrm{r}_1 \times 1} \\ 0_{\mathrm{r}_2 \times 1} & \boldsymbol{\lambda}_2 \end{bmatrix} = \begin{bmatrix} \left[\lambda_{01} \;\; \lambda_{11} \;\; \ldots \;\; \lambda_{\mathrm{r}_i - 1, 1}\right]^T & 0_{\mathrm{r}_1 \times 1} \\ 0_{\mathrm{r}_2 \times 1} & \left[\lambda_{02} \;\; \lambda_{12} \;\; \ldots \;\; \lambda_{\mathrm{r}_2 - 1, 2}\right]^T \end{bmatrix}, \end{aligned} \tag{19}$$

subsystem (17) is described by equation: $z^{(\mathrm{r})} + \boldsymbol{\lambda}^T Z = b_0(\hat{v} + \varepsilon), b_0 = \mathrm{diag}\left\{b_{01}, b_{02}\right\}$; if $z^{(\mathrm{r})} = \bar{z}^{(\mathrm{r})}$ and $Z = \bar{Z}$, the error $\varepsilon = \left[\varepsilon_1 \;\; \varepsilon_2\right]^T$ becomes $\varepsilon = 0_{2\times 1}$; for $b_0 = I_2$, $\lambda_{01} = \lambda_{11} = \lambda_{02} = \lambda_{12} = 0$, the following equation results:

$$\hat{v}_{\mathrm{r}} = \bar{z}^{(\mathrm{r})} + \boldsymbol{\lambda}^T \bar{Z} = \left[\dddot{\bar{Y}} + \lambda_{21}\ddot{\bar{Y}} \;\; \ddot{\bar{\beta}}\right]^T. \tag{20}$$

For $z_1 = Y$ ($\mathrm{r}_1$=3) and $z_2 = \beta$ ($\mathrm{r}_2$=2), choosing the transfer functions $H_{d_1}(\mathrm{s}) = \dfrac{b_{01}}{s^2(s + \lambda_{21})}, H_{d_2}(\mathrm{s}) = \dfrac{b_{02}}{s^2}$, there will be obtained null stationary errors $\left(Y_{st} = \dot{Y}_{st} = \beta_{st} = \dot{\beta}_{st}\right)$.

Now, taking into account the equation (12), $z^{(\mathrm{r})} + \boldsymbol{\lambda}^T Z$ becomes:

$$z^{(\mathrm{r})} + \boldsymbol{\lambda}^T Z = \begin{bmatrix} \dddot{Y} + \ddot{Y} \\ \ddot{\beta} \end{bmatrix} = \begin{bmatrix} a''_{61} & a''_{62} & a''_{63} & a''_{64} & 0 & 0 & a''_{67} & a''_{68} \\ a'_{11} & a'_{12} & a'_{13} & a'_{14} & 0 & 0 & a'_{17} & a'_{18} \end{bmatrix} \hat{x} + \begin{bmatrix} -\dfrac{V_0 b_{11}}{T_a} & -\dfrac{V_0 b_{12}}{T_r} \\ \dfrac{b_{11}}{T_a} & \dfrac{b_{12}}{T_r} \end{bmatrix} \hat{u} + \begin{bmatrix} a''_{31} & -a_{11} \\ -\dfrac{a'_{11}}{V_0} & \dfrac{a_{11}}{V_0} \end{bmatrix} \begin{bmatrix} w \\ \dot{w} \end{bmatrix}, \tag{21}$$

where, one has chosen $\lambda_{21} = b_{01} = 1$; $\hat{x}$ is the system estimated state, $a''_{61} = a''_{61} - V_0 a_{11}, a''_{62} = a'_{62} - V_0 a_{12}$, $a''_{63} = a'_{63} - V_0(a_{13} + 1), a''_{64} = a'_{64} - V_0 a_{14}, a''_{67} = a'_{67} - V_0 b_{11}, a''_{68} = a'_{68} - V_0 b_{12}$, and $a''_{31} = a'_{31} + 1$. Using the equations $z^{(\mathrm{r})} + \boldsymbol{\lambda}^T Z = b_0(\hat{v} + \varepsilon)$ and (21), identifying the terms of the pseudo-control $\hat{v}$ and error ε, we get:

$$\begin{aligned} &\hat{v} = \begin{bmatrix} \hat{v}_1 \\ \hat{v}_2 \end{bmatrix} = \begin{bmatrix} \hat{h}_{\mathrm{r}_1}(z, \hat{u}) \\ \hat{h}_{\mathrm{r}_2}(z, \hat{u}) \end{bmatrix} = \hat{h}_{\mathrm{r}}\left(\hat{Y}, \hat{\beta}, \hat{u}\right), \hat{u} = \begin{bmatrix} \hat{\delta}_{a_c} & \hat{\delta}_{r_c} \end{bmatrix}^T \Leftrightarrow \hat{v} = \begin{bmatrix} a''_{61} & 0 \\ 0 & a'_{11} \end{bmatrix} \begin{bmatrix} \hat{Y} \\ \hat{\beta} \end{bmatrix} + \begin{bmatrix} -\dfrac{V_0 b_{11}}{T_a} & -\dfrac{V_0 b_{12}}{T_r} \\ \dfrac{b_{11}}{T_a} & \dfrac{b_{12}}{T_r} \end{bmatrix} \begin{bmatrix} \hat{\delta}_{a_c} \\ \hat{\delta}_{r_c} \end{bmatrix} \Leftrightarrow \\ &\Leftrightarrow \hat{u} = \begin{bmatrix} \hat{\delta}_{a_c} \\ \hat{\delta}_{r_c} \end{bmatrix} = \hat{h}_{\mathrm{r}}^{-1}(\hat{z}, \hat{v}) = \begin{bmatrix} -\dfrac{V_0 b_{11}}{T_a} & -\dfrac{V_0 b_{12}}{T_r} \\ \dfrac{b_{11}}{T_a} & \dfrac{b_{12}}{T_r} \end{bmatrix}^{-1} \left( \hat{v} - \begin{bmatrix} a''_{61} & 0 \\ 0 & a'_{11} \end{bmatrix} \begin{bmatrix} \hat{Y} \\ \hat{\beta} \end{bmatrix} \right) \end{aligned} \tag{22}$$

and

$$\varepsilon = \begin{bmatrix} \varepsilon_1 \\ \varepsilon_2 \end{bmatrix} = \begin{bmatrix} a''_{62} & a''_{63} & a''_{64} & a''_{67} & a''_{68} \\ a'_{12} & a'_{13} & a'_{14} & a'_{17} & a'_{18} \end{bmatrix} \begin{bmatrix} \hat{p} & \hat{r} & \hat{\varphi} & \hat{\delta}_a & \hat{\delta}_r \end{bmatrix}^T + \begin{bmatrix} a''_{31} & -a_{11} \\ -\dfrac{a'_{11}}{V_0} & \dfrac{a_{11}}{V_0} \end{bmatrix} \begin{bmatrix} w \\ \dot{w} \end{bmatrix}; \tag{23}$$

in the previous equations $\hat{Y}, \hat{\beta}, \hat{p}, \hat{r}, \hat{\varphi}, \hat{\psi}, \hat{\delta}_a$, and $\hat{\delta}_r$ are the components of the estimated state vector $\hat{x}$. Using the Taylor series expansion of the function $\bar{u} = h_r^{-1}(z, v) = \hat{h}_r^{-1}(z, \hat{v}) + \dfrac{d}{dv}\left(h_r^{-1}(z, v)\right)_{v=\hat{v}}(v - \hat{v}) = \hat{h}_r^{-1}(z, \hat{v}) +$ $+ \dfrac{d}{d\hat{v}}\left(\hat{h}_r^{-1}(z, \hat{v})\right)\varepsilon$ and replacing the vector $z$ with its estimate $(\hat{z})$, according to the equation $\bar{u} = h_r^{-1}(z, v)$, $\hat{u} = h_r^{-1}(z, \hat{v})$, one gets:

$$\bar{u} = \hat{u} + \varepsilon \frac{d}{d\hat{v}}\left(h_r^{-1}(z, \hat{v})\right). \tag{24}$$

Replacing now $\hat{u}$ (form (22)) into equation (24), the final form of the control law $\bar{u}$ is obtained as follows:

$$\bar{u} = \begin{bmatrix} \bar{\delta}_{a_c} \\ \bar{\delta}_{r_c} \end{bmatrix} = \hat{h}_r^{-1}(\hat{z}, v) = \begin{bmatrix} -\dfrac{V_0 b_{11}}{T_a} & -\dfrac{V_0 b_{12}}{T_r} \\ \dfrac{b_{11}}{T_a} & \dfrac{b_{12}}{T_r} \end{bmatrix}^{-1} \left( v - \begin{bmatrix} a''_{61} & 0 \\ 0 & a'_{11} \end{bmatrix} \begin{bmatrix} \hat{Y} \\ \hat{\beta} \end{bmatrix} \right); \tag{25}$$

thus, the control law $\bar{u}$ may be directly calculated by means of (22), where $\hat{u}$ is replaced by $\bar{u}$ and $\hat{v}$ by $v = \hat{v} + \varepsilon$. The general control law $u$ has again the form (5), where the component $u_\infty$ (the component obtained by using the H-inf control) has the same form like the one in the case of the first landing system (the form of $u_\infty$ is (7) with $P_\infty$ – the stabilizing solution of the Riccati matriceal equation (8)).

*B. The structure of the second new automatic landing system for the approach phase*

The structure of the second new control system for aircraft guidance during the landing approach phase, using dynamic inversion, H-inf method, and a dynamic compensator is presented in Fig. 3. The vectors $\bar{z}$ and $\hat{v}_r$ are calculated by means of two reference models [5]; these are identical with the ones presented in Fig. 2 where, this time, $v_{h_1} = v_{h_2} = 0$ or $v_{h_1} \neq 0, v_{h_2} \neq 0$. The forms of the signals $v_{h_1}$ and $v_{h_2}$ (the two components of the Pseudo Control Hedging block's output - $v_h$) will be presented in the section 4.C. As in the case of the first control system (the one in Fig. 1), the desired landing trajectory of aircraft mainly involves the same two

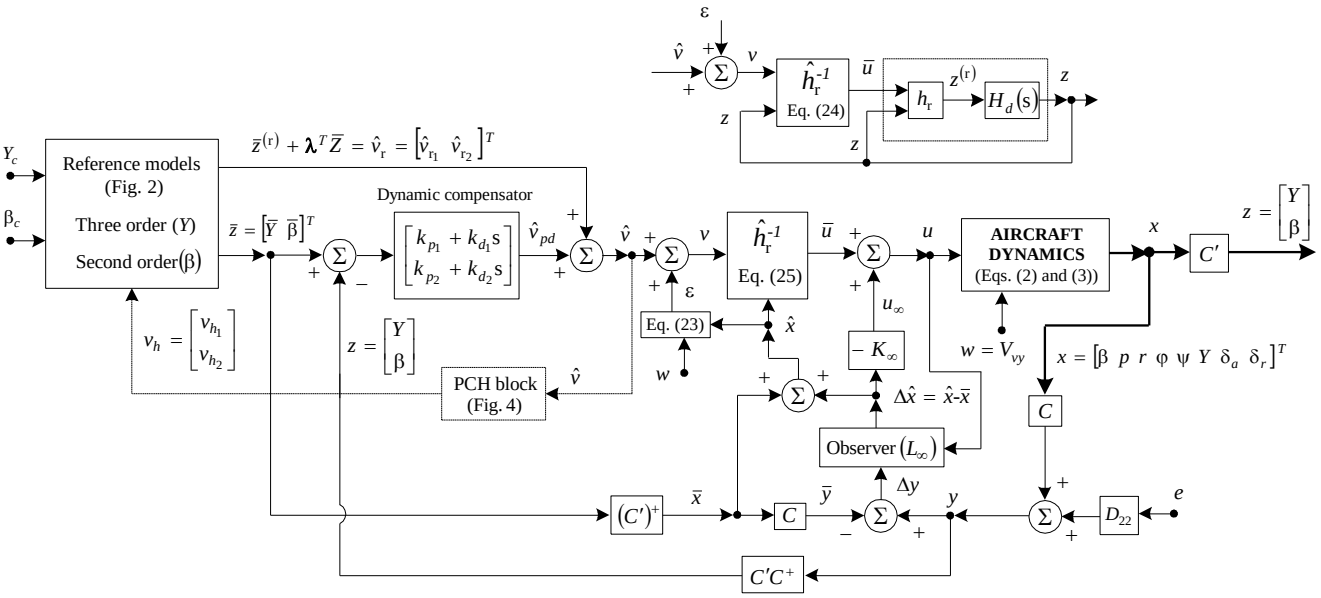


Fig. 3 The second ALS for the aircraft control in lateral plane using the H-inf control and the dynamic inversion

variables' control: the aircraft lateral deviation with respect to the runway and the sideslip angle. The ALS in Fig. 3 must assure the convergences: $y = Cx \to \bar{y} = C\bar{x}, x \to \bar{x}, z = C'x \to \bar{z} = C'\bar{x}, \hat{x} \to x \to \bar{x}, u_\infty \to 0$, $\bar{u} \to 0, u \to 0$.

The linear dynamic compensator is chosen as proportional-derivative (PD) one; it provides the signal $\hat{v}_{pd}$ – necessary for the system's stabilization. The proportional coefficients ($k_{p_1}$ and $k_{p_2}$) and the derivative ones ($k_{d_1}$ and $k_{d_2}$) associated to the dynamic compensator are calculated by imposing desired roots (solutions) for the characteristic equations of the linear closed loop subsystem with unitary and negative feedback (the system having on the direct way the transfer matrix $H_d$(s)); the control signal $u_\infty$ is neglected during this step. The two characteristic equations are: $s^3 + \lambda_{21}s^2 + b_{01}s + b_{01}k_{p_1} = 0$ and $s^2 + (b_{02}k_{d_2} + \lambda_{12})s + b_{02}k_{p2} = 0$, respectively; we have chosen $\lambda_{21}=b_{01}=b_{02}=1$ and $\lambda_{12}=0$. Thus, the parameters of the dynamic compensator are calculated such that the two characteristic equations presented above have imposed (desired) solutions, i.e. all the complex solutions are placed in the left-hand side of the complex plane. Without loosing the generality, these solutions can be the same with the poles of the reference models' transfer functions.

*C. The structure of the Pseudo Control Hedging block*

The controllers are sometimes sensitive to actuators' nonlinearities; that is why, in the architecture of these controllers, one may introduce a block which limits the pseudo-control by means of a component representing an estimation of the execution element's dynamics (PCH - Pseudo Control Hedging) [29]. The input saturation and the input rate saturation may also be significant problems; the saturation violates the assumption of affinity in control and the assumption that the sign of the effect of the control is known/non-zero, since the effect of additional control input is zero once saturation is entered. The main purpose of the Pseudo Control Hedging (PCH) control method is to prevent the adaptive element of a control system from trying to adapt to a class of system input characteristics (characteristics of plant or of the controller). To achieve this issue, the control law is prevented from "seeing" the system characteristic. A plain-language conceptual description of the method belongs to Johnson and Calise: *The reference model is moved backwards (hedged) by an estimate of the amount the plant did not move due to system characteristics the control designer does not want the adaptive control element to 'know' about*. In other words, in the context of a control law involving dynamic inversion, "movement" should be replaced by some system signal. Preventing the adaptive element from "knowing" about a system's characteristics means to prevent that adaptive element from seeing the system characteristic as model tracking error [30]. On the other hand, the adaptive controllers are sensitive to actuator nonlinearity. That is why, in these controllers' architecture, one may introduce a block which limits the pseudo-control by means of a component (PCH) representing an estimation of the execution element's dynamics. In this paper, we introduce a PCH block which limits the signal $v$ with a component representing the actuator dynamics' estimation. Thus, PCH "moves back" the reference model, introducing a reference model's response correction with respect to the estimation of the execution element's position. The signal provided by PCH $v_h = \begin{bmatrix} v_{h_1} & v_{h_2} \end{bmatrix}^T$ is a reference model's additional input [29, 30]. The block diagrams for the modeling of the servo-ailerons, servo-rudder, and the two components of the PCH block's output ($v_{h_1}$ and $v_{h_2}$) are presented in Fig. 4. The equations that lead to these two block diagrams have resulted by using the equations (22). Thus, by means of (22), one obtained:

$$\begin{aligned} \hat{v}_1 &= a''_{61}\hat{Y} - \frac{V_0 b_{11}}{T_a}\hat{\delta}_{a_c} - \frac{V_0 b_{12}}{T_r}\hat{\delta}_{r_c} \cong a''_{61}\hat{Y} - \frac{V_0 b_{11}}{T_a}\hat{\delta}_{a_c} = \hat{h}_{r_1}(z, \hat{u}), \\ \hat{v}_2 &= a'_{11}\hat{\beta} + \frac{b_{11}}{T_a}\hat{\delta}_{a_c} + \frac{b_{12}}{T_r}\hat{\delta}_{r_c} \cong a'_{11}\hat{\beta} + \frac{b_{12}}{T_r}\hat{\delta}_{r_c} = \hat{h}_{r_2}(z, \hat{u}); \end{aligned} \tag{26}$$

in the above two equations, we considered two independent channels (roll and yaw) and, that is why, we neglected the terms $(-V_0 b_{12}/T_r)\hat{\delta}_{r_c}$ and $(b_{11}/T_a)\hat{\delta}_{a_c}$ from the first and from the second equations (26), respectively. From (26) it can be easily obtained:

$$\delta_{a_c} \cong \hat{\delta}_{a_c} = \hat{h}_{r_1}^{-1}\left(\hat{Y}, \hat{v}_1\right) = \frac{T_a}{V_0 b_{11}}\left(a''_{61}\hat{Y} - \hat{v}_1\right), \quad \delta_{r_c} \cong \hat{\delta}_{r_c} = \hat{h}_{r_2}^{-1}\left(\hat{\beta}, \hat{v}_2\right) = \frac{T_r}{b_{12}}\left(-a'_{11}\hat{\beta} + \hat{v}_2\right). \tag{27}$$

Using now again equations (26), with some changes ($\hat{v}_1$ becomes $\bar{v}_1$ and $\hat{v}_2$ becomes $\bar{v}_2$), the following equations have resulted:

$$\bar{v}_1 = a''_{61}\hat{Y} - \frac{V_0 b_{11}}{T_a}\bar{\delta}_a, \quad \bar{v}_2 = a'_{11}\hat{\beta} + \frac{b_{12}}{T_r}\bar{\delta}_r. \tag{28}$$

The two components of the PCH block's output ($v_{h_1}$ and $v_{h_2}$) will have the forms: $v_{h_1} = \hat{v}_1 - \bar{v}_1$ and $v_{h_2} = \hat{v}_2 - \bar{v}_2$, respectively.

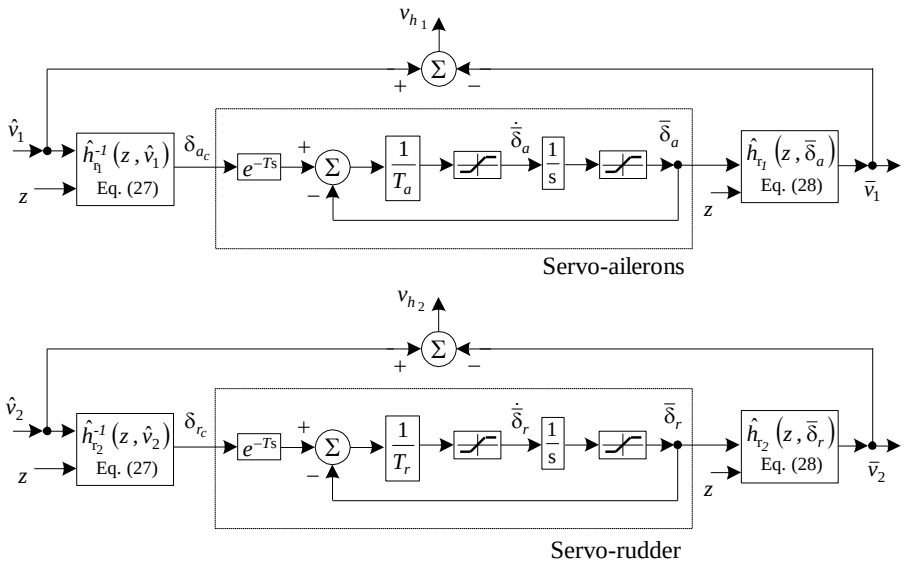


Fig. 4 The block diagrams for the modeling of the servo-ailerons, servo-rudder, and the two components of the PCH block's output

## 5. Numerical Simulation Results

*A. Numerical simulation setup*

To study the performances of the new obtained automatic landing systems, we consider the landing approach phase of a light airplane (Charlie airplane). Complex simulations in Matlab/Simulink environment have been performed; thus, one designed the optimal observers, the H-inf controllers, and, after that, validated the proposed automatic landing systems in lateral-directional plane.

The values of the coefficients for Charlie light airplane's landing dynamics have been borrowed from [5]: $a_{11} = -0.0013, a_{12} = 0, a_{13} = -1, a_{14} = 0.15, a_{21} = -1.33, a_{22} = -0.98, a_{23} = 0.33, a_{31} = 0.17, a_{32} = -0.17, a_{33} = -0.217, b_{11} = 0.001, b_{12} = 0.015, b_{21} = 0.23, b_{22} = 0.06, b_{31} = 0.026, b_{32} = -0.15, V_0 = 67\,\text{m/s}, T_a = 0.7\,\text{s}, T_r = 0.1\,\text{s}, \mu_1 = 1, \mu_2 = 1, c_1 = c_2 = 0.01, \bar{Y} = 0\,\text{m}, \bar{\beta} = 0\,\text{deg}$; the vector $e$ is $e = [0\,\text{m}\ \ 0\,\text{m/s}\ \ 1\,\text{deg}\ \ 0\,\text{deg}\ \ 1\,\text{deg/ s}\ \ 0\,\text{deg}\ \ 1\,\text{deg/ s}]^T$, the matrix $G$ has been obtained by means of equation (3), while the system's initial state is $x(0) = [0.1\,\text{deg}\ \ 0\,\text{deg/ s}\ \ -2\,\text{deg/ s}\ \ 0\,\text{deg}\ \ 0.1\,\text{deg}\ \ 25\,\text{m}\ \ 0\,\text{deg}\ \ 0\,\text{deg}]^T$; for the reference models, we have chosen: $p = 25, \xi_1 = \xi_2 = 0.7, \omega_1 = \omega_2 = 2\,\text{rad/s}$. To test the robustness of the two new ALSs with respect to the crosswind (lateral wind - $V_{vy}$), in the simulations there will be considered different values for $w = V_{vy}$ between 2 m/s and 10 m/s. The values considered in this paper for the sensors' errors are chosen very large because it is important to use strong disturbances instead of small ones when designing a robust ALS.

*B. Results and discussion for the first flight control system during the landing approach phase*

One has solved the Riccati equations (8) and (9); it resulted $P_\infty$ and $P_\infty^*$; the calculation of the gain

matrices $K_\infty$ and $L_\infty$ is made by means of (7) and $L_\infty = P_\infty^* C^T \left(D_{22}^T D_{22}\right)^{-1}$, respectively. The form of the command law $\bar{u}$ resulted from (13); one has software implemented the block diagram in Fig. 1 and obtained the observer estimation errors, the main variables' time history, and the influence of crosswind upon the aircraft lateral deviation with respect to the runway ($Y$) and the sideslip angle ($\beta$).

$$P_\infty = \begin{bmatrix} 95.28 & 0.37 & -23.60 & 2.14 & -92.81 & -5.08 & -0.007 & 0.26 \\ 0.37 & 0.14 & -0.09 & 0.18 & -0.03 & -0.007 & 0.01 & 0.002 \\ -23.60 & -0.09 & 8.09 & -0.50 & 24.11 & 1.01 & 0.02 & -0.09 \\ 2.14 & 0.18 & -0.50 & 0.29 & -1.43 & -0.07 & 0.02 & 0.007 \\ -92.81 & -0.03 & 24.11 & -1.43 & 95.59 & 5.09 & 0.04 & -0.26 \\ -5.08 & -0.007 & 1.01 & -0.07 & 5.09 & 0.39 & 0 & -0.01 \\ -0.007 & 0.01 & 0.02 & 0.02 & 0.04 & 0 & 0.002 & 0 \\ 0.26 & 0.002 & -0.09 & 0.007 & -0.26 & -0.01 & 0 & 0.001 \end{bmatrix}, P_\infty^* \cong \begin{bmatrix} 0.03 & -0.001 & -0.008 & 0 & 0.01 & -0.007 & 0 & 0 \\ -0.001 & 0.005 & 0.002 & 0.005 & -0.001 & 0 & 0 & 0 \\ -0.008 & 0.002 & 0.004 & 0.002 & -0.007 & 0 & 0 & 0 \\ 0 & 0.005 & 0.002 & 0.006 & 0 & 0 & 0 & 0 \\ 0.01 & -0.001 & -0.007 & 0 & 0.03 & 0.007 & 0 & 0 \\ -0.007 & 0 & 0 & 0 & 0.007 & 0.01 & 0 & 0 \\ 0 & 0 & 0 & 0 & 0 & 0 & 0 & 0 \\ 0 & 0 & 0 & 0 & 0 & 0 & 0 & 0 \end{bmatrix},$$

$$K_\infty = \begin{bmatrix} -1.020 & 264.615 \\ 2.606 & 2.318 \\ 3.304 & -96.359 \\ 3.189 & 7.411 \\ 5.996 & -266.363 \\ 0.059 & -10.771 \\ 0.388 & -0.176 \\ -0.02 & 1.173 \end{bmatrix}^T, L_\infty = 10^{-4} \begin{bmatrix} -0.19 & -24.99 & 0.76 & 0.01 & -0.03 & 0.38 & -0.2 \\ -0.01 & -0.49 & -0.03 & 0.14 & 0.13 & -0.04 & 0.07 \\ 0 & 0.44 & -0.2 & 0.06 & 0.07 & -0.2 & 0.11 \\ 0 & -0.03 & 0.01 & 0.15 & 0.14 & 0.01 & 0.06 \\ 0.19 & 25 & 0.28 & 0.01 & -0.04 & 0.76 & -0.2 \\ 0.37 & 25 & -0.19 & 0 & -0.01 & 0.19 & 0 \\ 0 & 0 & -0.02 & 0.02 & 0.02 & -0.02 & 0.02 \\ 0 & 0 & 0 & 0 & 0 & 0 & 0 \end{bmatrix}.$$

In Fig. 5 the observer estimation errors are presented for aircraft's lateral-directional motion (landing approach phase); the optimal observer is convergent - all the 8 components of the state $\Delta\hat{x} = \hat{x} - \bar{x}$ tend to zero in about 5 seconds. The results are the same whether the sensor errors are taken or not into consideration. In Fig. 6 we represent the time characteristics for the flight direction control system (Fig. 1); before the start of the two landing main stages in longitudinal plane, the pilot must cancel aircraft's lateral deviation with respect to the runway. The characteristics have been represented for the first ALS affected by crosswind ($V_{vy}$=2 m/s) in the presence or in the absence of sensor errors (the sensors are used for the measurement of the states). The presence of the sensor errors is not visible – the curves with solid line (obtained for the first ALS without sensor errors) overlap almost perfectly over the curves plotted with dashed line (obtained for the first ALS with sensor errors).

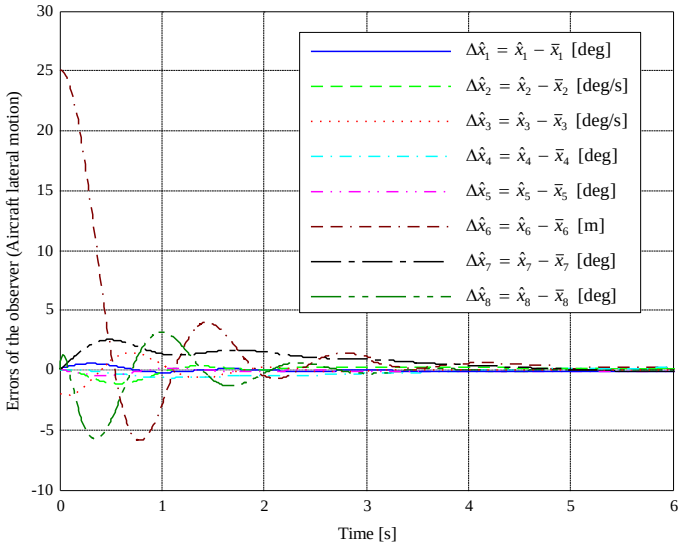


Fig. 5 State estimation errors by using the optimal observer for the aircraft lateral motion

The landing approach begins at the nominal speed (67 m/s); the speed should be maintained constant. To test the robustness of the first designed ALS, in all simulations, we have taken into consideration the

crosswind, because low-altitude crosswind can be a serious threat to the safety of aircraft in landing. From 6th mini-graphic in Fig. 6 (achieved for $V_{vy}$=2 m/s), we can see that the stationary value of the aircraft lateral deviation ($Y$) is very close to zero; this error is very good if we analyze the Federal Aviation Administration (FAA) accuracy requirements for Category III (best category) [31]; according to FAA Category III accuracy requirements, the lateral error must be less than 4.1 m. If the lateral error is between 4.1 m and 4.6 m, the aircraft meets the Category II precision standards, while if the lateral error is between 4.6 m and 9.1 m, the aircraft meets Category I precision standards. The used technique (H-inf control) can handle the plant with measurement noise (sensor errors) and crosswind. If the crosswind is stronger than its maximum accepted value, the pilot must avoid having the aircraft enter into this wind shear. From the sideslip angle's point of view, the errors are less than 0.01 deg.; we conclude that $\beta \rightarrow \beta_c$=0 deg. We also tested the first designed ALS for different values of the crosswind (between 2 m/s and 10 m/s) in order to analyze the system's robustness when the lateral wind has medium or high values. Thus, in Fig. 7 we represent the time history of the main two control variables ($Y$ and $\beta$) for different values of the lateral wind. As one can see from the time characteristics in Fig. 7, the errors $Y$-$Y_c$ and $\beta$- $\beta_c$ increase together with the value of the crosswind, i.e. the error with respect to $Y$ is 0.75 m for $V_{vy}$=2 m/s, 1.48 m for $V_{vy}$=4 m/s, 2.21 m for $V_{vy}$=6 m/s, 2.96 m for $V_{vy}$=8 m/s, and 3.69 m for $V_{vy}$=10 m/s; the errors meet the FAA accuracy requirements for Category III, although the lateral wind take even large values. On the other hand, the errors with respect to $\beta$, for different values of the lateral wind, are very small (less than -0.027 deg).

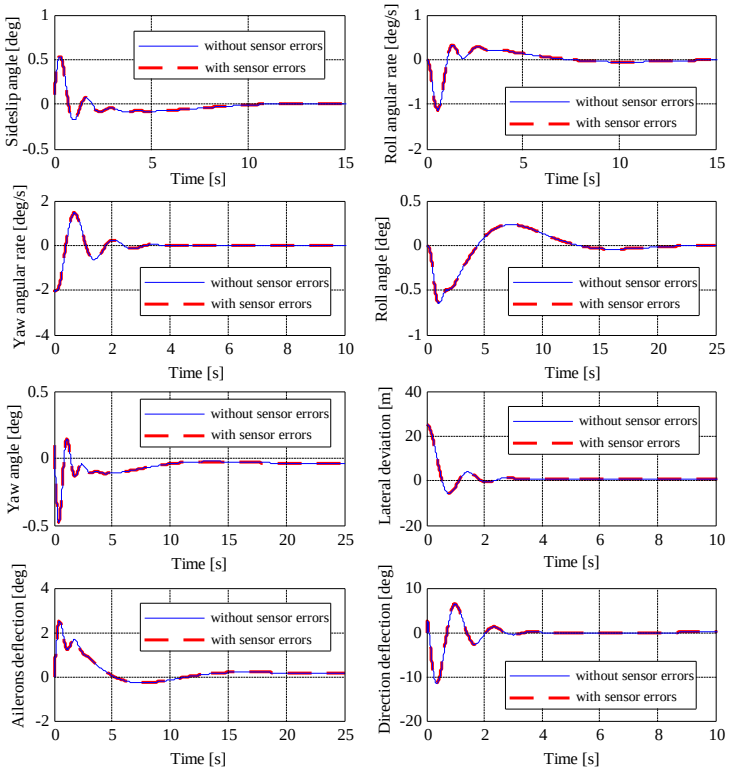


Fig. 6 Time characteristics of the first lateral-directional control system, with or without sensor errors

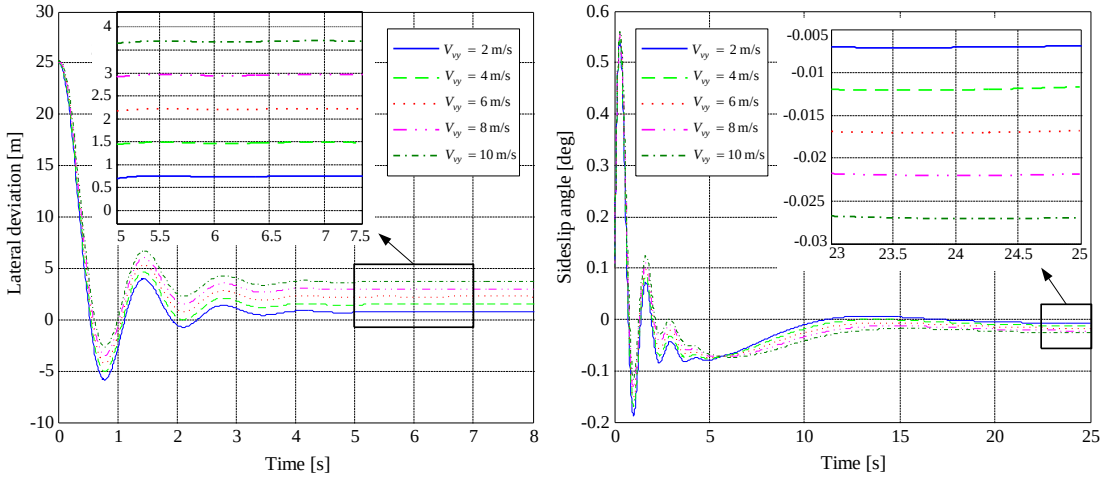


Fig. 7 Time history of the main two control variables for different values of the lateral wind (first ALS)

*C. Results and discussion for the second flight control system during the landing approach phase*

For the second control system (Fig. 3), the data that lead to the obtaining of the matrices $P_\infty$, $P_\infty^*$, $K_\infty$, $L_\infty$ are the same; that is why, these matrices are the same with the ones obtained in the previous sub-section of the paper. The form of the signal $u_\infty$ is again (7), while the control signal $\bar{u}$ is calculated by means of the equation (25). Also, we software implemented the block diagram in Fig. 3 and obtained the observer's estimation errors, the main variables' time history, and the influence of crosswind upon the aircraft lateral deviation with respect to the runway (*Y*) and the sideslip angle (β); moreover, we will analyze the influence of Pseudo Control Hedging usage in the case of nonlinear actuators.

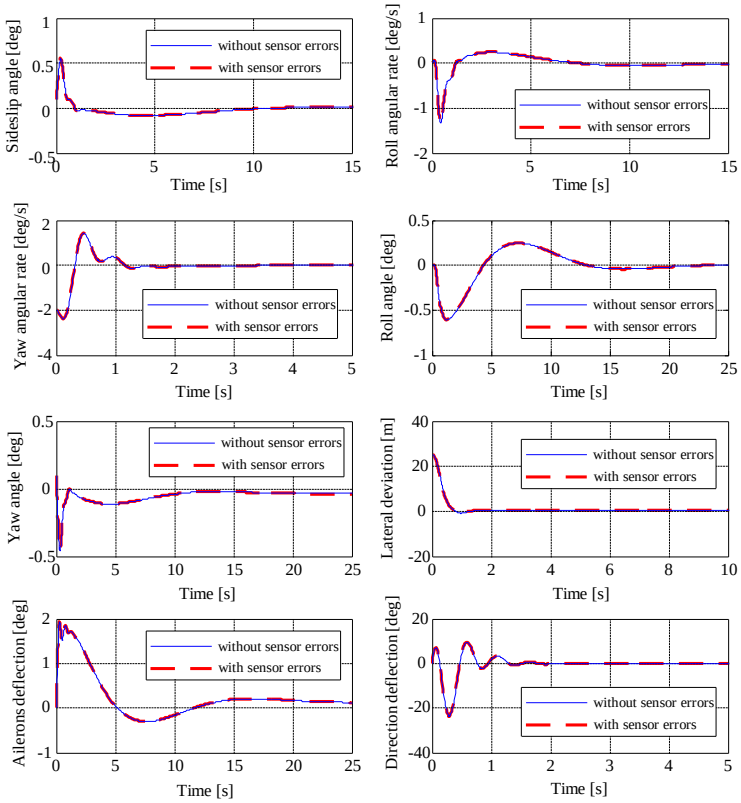


Fig. 8 Time characteristics of the second lateral-directional control system, with linear actuators, with or without sensor errors

The time history of the observer estimation errors is similar to the one in Fig. 5 for the aircraft lateral-directional motion (landing approach phase); the same conclusion can be drawn regarding the convergence of the optimal observer and its convergence speed. In Fig. 8 we represented the time characteristics for the

flight direction control system (Fig. 3); the characteristics have been represented for the second control system affected by low crosswind ($V_{vy}$=2 m/s), with linear actuators ($\nu_h$=0), in the presence or in the absence of sensors' errors. The same conclusion can be drawn regarding the overlap of the curves with solid line and the curves plotted with dashed line.

We also tested this second designed ALS (lateral-directional motion), with linear actuators ($\nu_h$=0), for different values of the crosswind (between 2 m/s and 10 m/s) in order to analyze the system's robustness when the lateral wind has medium or high values. Thus, in Fig. 9 we represented the time history of the main two control variables ($Y$ and β) for different values of the lateral wind. Analyzing Fig. 9, one can conclude that the errors $Y$-$Y_c$ and β- $\beta_c$ increase together with the value of the crosswind; for example, the error with respect to $Y$ is 0.58 m for $V_{vy}$=2 m/s, 1.21 m for $V_{vy}$ =4 m/s, 1.85 m for $V_{vy}$ =6 m/s, 2.50 m for $V_{vy}$ =8 m/s, and 3.14 m for $V_{vy}$ =10 m/s, respectively; all the errors meet the FAA accuracy requirements for Category III, although the lateral wind take even large values. On the other hand, the errors with respect to β, for different values of the lateral wind, are very small (less than -0.02 deg). It is very important to remark that all these errors (both for $Y$ and β) are smaller than their homologues in the case of the first ALS; other remarks regarding the comparison between the two new lateral-directional control systems will be presented in the next sub-section of this paper.

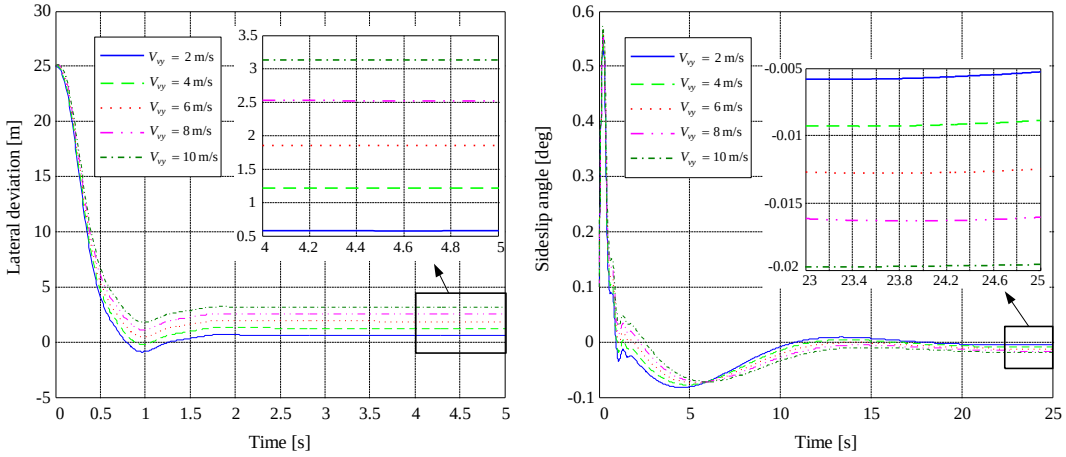


Fig. 9 Time history of the main two control variables for different values of the lateral wind (second ALS with linear actuators)

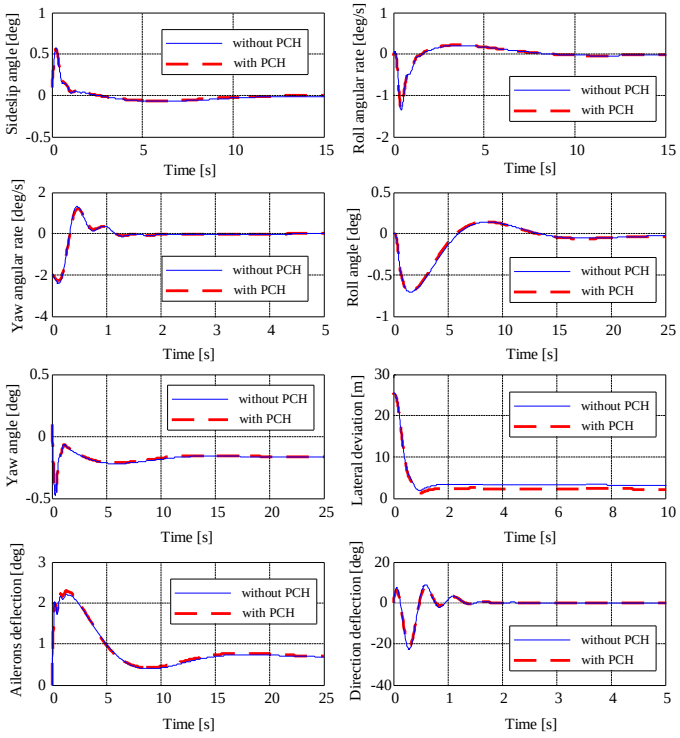


Fig. 10 Time characteristics of the second lateral-directional control system, with nonlinear actuators, with or without PCH

The second designed system works both with linear and nonlinear actuators. In real cases, the actuators of the system may be close to linear or nonlinear actuators' models. Usually, the real actuators are closer to the nonlinear models because the deflection angles and the angular rates are limited and, furthermore, these actuators are characterized by a delay time. If the actuators are linear, their modeling equations are the last two equations (1); for this case the characteristics in Fig. 8 have been obtained.

If the actuators are nonlinear, their models are the ones presented in Fig. 4; in this case, it is good to use a PCH block $(v_h \neq 0)$, because it allows the system to work in the linear zones of the nonlinearities. As we already presented in the fourth section of this paper, the signal provided by the PCH block $v_h = \begin{bmatrix} v_{h_1} & v_{h_2} \end{bmatrix}^T$ is a reference model's additional input. In the case of nonlinear actuators, we analyze the influence of Pseudo Control Hedging usage on the second ALS's variables, by representing in Fig. 10 the time characteristics for the second flight direction control system with nonlinear actuators, affected by large crosswind ($V_{vy}$=10 m/s), in the presence of the sensors' errors, taking or not into account the signals from the PCH block.

Analyzing Fig. 10, we can remark that the usage of a PCH block improves the system's behavior; this is obvious especially in the case of the lateral deviation *Y*. In order to emphasize this, we plotted in Fig. 11 the time history of the lateral deviation with respect to the runway (*Y*), for different values of the lateral wind, using or not a PCH block when the actuators are nonlinear. Thus, from Fig. 11 we conclude that the differences between the dashed line curves (*Y* with PCH) and the solid line ones (*Y* without PCH) are easier to seen for large values of the crosswind; thus, the difference between the two curves is 0.25 m for $V_{vy}$=4 m/s, 0.3 m for $V_{vy}$ =6 m/s, 0.4 m for $V_{vy}$ =8 m/s, and 0.5 m for $V_{vy}$ =10 m/s, respectively. This means that, in the case of nonlinear actuators' usage, the PCH block decreases the lateral deviation error, especially for large values of the crosswind, this improving the quality of the aircraft lateral-directional control system.

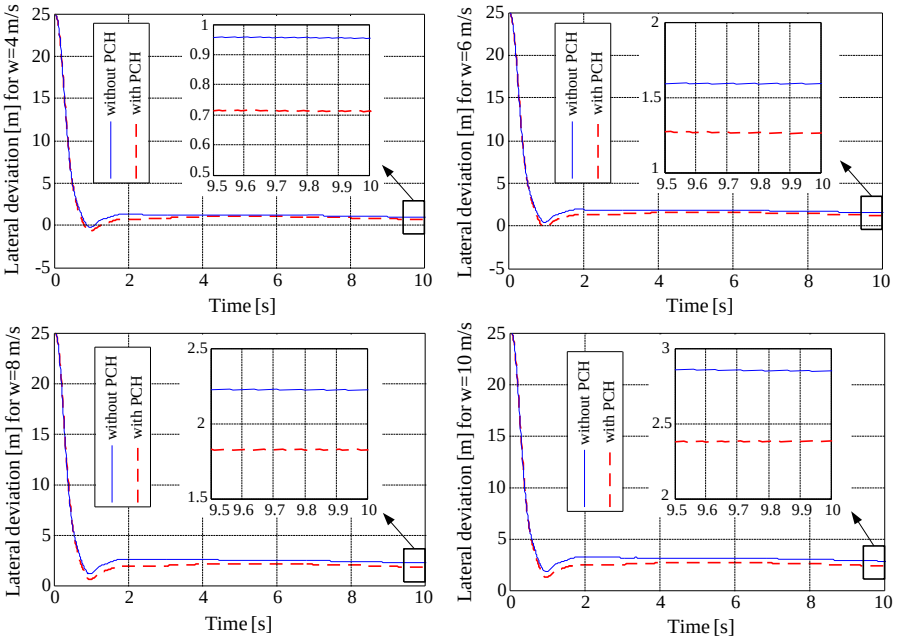


Fig. 11 Aircraft lateral deviation (*Y*), for different values of the lateral wind, using or not a PCH block

*D. Comparison between the two new lateral-directional control systems*

For the two lateral-directional control systems (the ones in Fig. 1 and in Fig. 3), Fig. 12 exposes the main two control variables (*Y* and β), for different values of the lateral wind; as one can see, the second ALS (ALS-2) is characterized by better quality indicators (damping, overshoots, stationary values, and transient regime periods). In Table 1 a comparison, for *Y* and β, between the overshoot (OVS), the transient regime period (TRP), and the stationary value (SV) for the two variants of ALS is achieved. From the TRP's point of view, the values are approximately the same for β, while, for *Y*, the ALS-2/ALS-1 improvement ratio is: 1.9 times; from the OVS's point of view, the ALS-2/ALS-1 improvement ratio is appreciatively 5.37 times for *Y* and appreciatively 2.125 for β. From the stationary values' point of view,

we also remark the advantages of ALS-2 with respect to ALS-1; thus, for *Y*: a decrease from 0.42 m to 0.30 m for w=2 m/s, a decrease from 1.13 m to 0.90 m for w=4 m/s, a decrease from 1.9 m to 1.59 m for w=6 m/s, and a decrease from 2.65 m to 2.21 m for w=8 m/s, while, for β, the decreases are also evident although these are characterized by very small values. Taking into account all the above presented issue, we can conclude the superiority of the ALS-2 (Fig. 3) with respect to ALS-1 (Fig. 1). Both control systems have very good properties and meet the FAA best Landing Category, but, due to its better precision, ALS-2 can be used to control the lateral-direction motion of aircraft during the last two stages of landing (glide slope phase and flare phase), while ALS-1 can be used to control the lateral-direction motion of aircraft during the landing approach phase. The first presented ALS is easier to design, while the advantage of the ALS-2 is related to its better quality indicators and to the fact that this automatic landing system is more appropriate for the cases when the aircraft dynamics is strongly nonlinear.

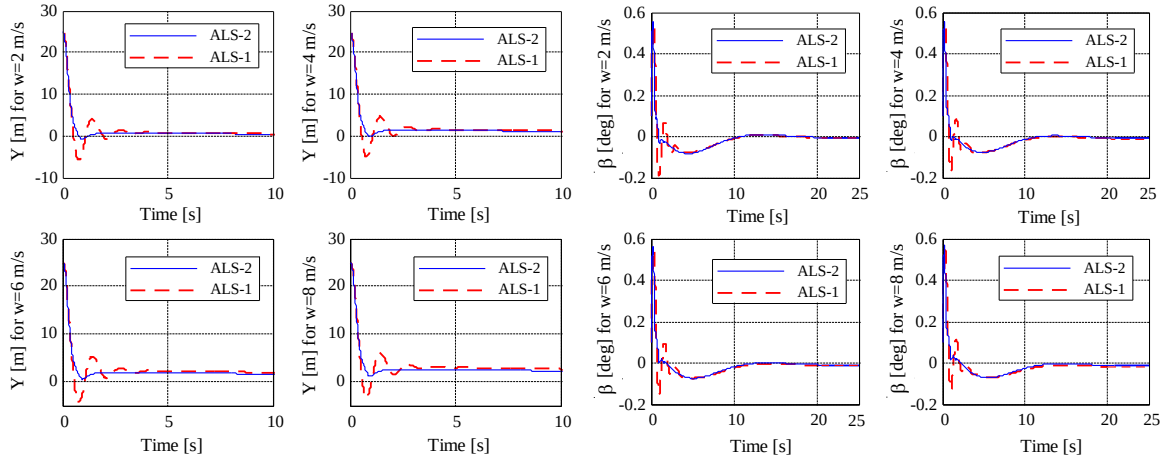


Fig. 12 Comparison between ALS-1 and ALS-2 for different values of the lateral wind

**Table 1 – Quality indicators for the ALSs in Fig. 1 and Fig. 3**

| **Variable** | | **Lateral deviation (*Y*)** | | | **Sideslip angle (β)** | | |
|---|---|---|---|---|---|---|---|
| **Quality indicators** | | **OVS** [m] | **TRP** [s] | **SV** [m] | **OVS** [deg] | **TRP** [s] | **SV** [deg] |
| ALS-1 (Fig. 1) | *w*=2 m/s | 6.32 | 3.5 | 0.42 | 0.19 | 15 | $-6.8 \cdot 10^{-3}$ |
| | *w*=4 m/s | 6.23 | | 1.13 | 0.17 | | $-11 \cdot 10^{-3}$ |
| | *w*=6 m/s | 6.20 | | 1.9 | 0.155 | | $-16 \cdot 10^{-3}$ |
| | *w*=8 m/s | 6.15 | | 2.65 | 0.135 | | $-21 \cdot 10^{-3}$ |
| ALS-2 (Fig. 3) | *w*=2 m/s | 1.31 | 1.8 | 0.30 | 0.085 | 15 | $-5.5 \cdot 10^{-3}$ |
| | *w*=4 m/s | 1.16 | | 0.90 | 0.080 | | $-8 \cdot 10^{-3}$ |
| | *w*=6 m/s | 1.14 | | 1.59 | 0.075 | | $-12 \cdot 10^{-3}$ |
| | *w*=8 m/s | 1.10 | | 2.21 | 0.071 | | $-15 \cdot 10^{-3}$ |

## 6. Conclusions

The purpose of this study was to design robust automatic landing systems for lateral-directional plane by using the H-inf control and the dynamic inversion technique. The H-inf method can handle both robustness and exact tracking problem, being very suited for the design of automatic landing systems. This technique provides robust stability with respect to the uncertainties caused by different disturbances and noise type signals, while the dynamic inversion provides good precision tracking. The new obtained systems represent extensions of the automatic landing system designed in [4], where only the landing in longitudinal plane is analyzed; our new automatic landing systems have some additional elements with respect to the one presented in [4]: an optimal observer, two reference models (which provide the desired lateral deviation with respect to the runway and the desired sideslip angle), and a dynamic compensator (only for the second designed ALS) which provides one of the control law components (the pseudo-command signal). The two calculation methods for the optimal control laws are characterized by a high degree of generality, applicability, and

simplicity. The simulation results are promising and show the robustness of the designed control systems even in the presence of crosswind and sensor errors; moreover, the very good errors meet the FAA accuracy requirements for Category III. On the other hand, the designed control laws have the ability to reject the measurement noise from sensors and the crosswind. Compared to other existing approaches in the field of ALSs, our method achieved higher tracking precision.

## References


[1] Lungu R, Lungu M, Grigorie TL. Automatic control of aircraft in longitudinal plane during landing. *IEEE Transactions on Aerospace & Electronic Systems*, 2013; **49** (2): 1338-1350.

[2] Singh S, Padhi R, Automatic Path Planning and Control Design for Autonomous Landing of UAVs using Dynamic Inversion, *American Control Conference Riverfront*, St. Louis, MO, USA , 2009; 2409-2414.

[3] Juang JG, Cheng KC. Application of Neural Network to Disturbances Encountered Landing Control, *IEEE Transactions on Intelligent Transportation Systems*, 2006; **7** (4): 582-588.

[4] Che J, Chen D. Automatic Landing Control using H-inf control and Stable Inversion, *Proceedings of the 40th Conference on Decision and Control*, Orlando, Florida, USA, 2001; 241-246.

[5] Sadati H, Sabzeh Parvar M, Menhaj MB. Comparison of Flight control Systems Design Methods in Landing, *Asian Journal of Control*, 2007; **9** (4): 491-496.

[6] Pashilkar A, Sundararajan N, Saratchhandran PA. Fault-Tolerant Neural Aided controller for Aircraft Auto-Landing, *Aerospace Science and Technology*, 2006; **10** (1): 49-61.

[7] Yuebang H, Hailong P, Tairen S. Robust Tracking Control of Helicopters using Backstepping with Disturbance Observers, *Asian Journal of Control*, 3013, DOI:10.1002/asjc.827.

[8] Yu GR. Nonlinear Fly-By-Throttle H-inf Control using Neural Networks, *Asian Journal of Control*, 2001; **3** (2): 163-169.

[9] Mori R, Suzuki S. Neural Network Modeling of Lateral Pilot Landing Control, *Journal of Aircraft*, 2009; **46**: 1721-1726.

[10] Vo H, Sridhar S. Robust Control of F-16 Lateral Dynamics, *International Journal of Aerospace and Mechanical Engineering* 2008; 80-85.

[11] Zdenko K, Stjepan B. *Fuzzy Controller Design – Theory and applications*, Taylor and Francis Group, 2006.

[12] Tsai, CC, Wang ZC, Lee CT, Li Y. Intelligent Adaptive Trajectory Tracking Control for an Autonomous Small-Scale Helicopter using Fuzzy Basis Function Networks, *Asian Journal of Control*, 2014, DOI: 10.1002/asjc.881.

[13] Shue S, Agarwal RK. Design of automatic landing systems using mixed $H_2/H_\infty$ control, *Journal of Guidance, Control, and Dynamics*, 1999; **2**: 103-114.

[14] Ochi Y, Kanai K. Automatic approach and landing for propulsion controlled aircraft by H∞ control *Proceedings of the 1999 IEEE International Conference on Control Applications*, Hawaii, 1999; 997-1002.

[15] Nho K, Agarwal RK. Automatic landing system design using fuzzy logic, *Journal of Guidance, Control and Dynamics*, 2000; **23**: 298-304.

[16] Juang JG, Chio, JZ. Fuzzy modelling control for aircraft automatic landing system, *International Journal of Systems Science*, 2005; **36** (2): 77-87.

[17] Asai S, Onuma H, Hata T, Miyazawa Y, Izumi T. Development of flight control system for automatic landing flight experiment, *Mitsubishi Heavy Ind. Techn. Rev.*, 1997; **34**: 112-124.

[18] Juang J, Chang H, Chang W. Intelligent automatic landing system using time delay neural network controller, *Applied Artificial Intelligence: An International Journal*, 2003; **17** (7): 563-581.

[19] Jourdan C, Marc C. Ground-Effect Identification and Autoland System Validation from Flight Data, *Journal of Aircraft*, 2004; **41** (4): 730-734.

[20] Malaek M, Izadi H, Pakmehr M. Flight Envelope Expansion in Landing Phase Using Classic, Intelligent and Adaptive Controllers, *Journal of Aircraft*, 2006; **43** (1): 91-101.

[21] Hall GW, Boothe EM. An in-flight investigation of lateral-directional dynamics for the landing approach, *Final technical Rept., Cornell Aeronautical Lab Inc Buffalo NY*, 1970.

[22] Parkinson BW, O'Connor ML, Fitzgibbon KT. Aircraft automatic approach and landing using GPS, *Global Positioning System: Theory and Applications*, 1996; **II**: 397-425.

[23] Lau K, Lopez R, Onate E. Neural Networks for Optimal Control of Aircraft Landing Systems, *Proceedings of the World Congress on Engineering*, 2007; **II**: 904-911.

[24] Kirk DE. *Optimal Control Theory. An Introduction*, Prentice Hall, 1970.

[25] Stoica AM. *Disturbance Attenuation and its Applications*, Romanian Academy Publisher, 2004.

[26] Calise AJ, Hovakymyan N, Idan M. Output Control of Nonlinear Systems Using Neural Networks, *Automatica*, 2001; 37 (8): 1201-1211.
[27] Isidori A. *Nonlinear Control Systems*, Springer Publisher, Berlin, 1995.
[28] Lungu R, Lungu M, Rotaru C. Non-linear adaptive system for the control of the helicopters pitch's angle. *Proceedings of the Romanian Academy, Series A: Mathematics, Physics, Technical Sciences, Information Science*, 2011; **12** (2): 133-142.
[29] Calise AJ, Johnson EN, Johnson MD, Corban JE. Applications of Adaptive Neural – Networks Control to Unmanned Aerial Vehicles, *Journal of Harbin Institute of Technology*, 2006; **38** (11): 1865-1869.
[30] Johnson EN, Calise AJ. Pseudo – Control Hedging: A New Method for Adaptive Control, *Navigation Guidance and Control Technology Workshop*, November 1-2, 2000.
[31] Braff R, Powell JD, Dorfler J. Applications of GPS to air traffic control, *Global Positioning System: Theory and Applications*, 1996; **II**: 327-374.